

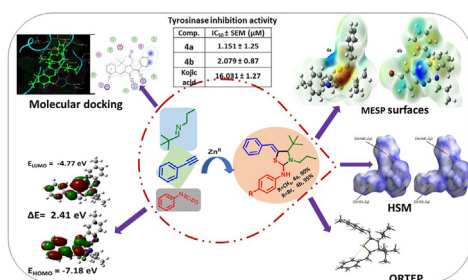


Research article

Identification of two novel thiazolidin-2-imines as tyrosinase inhibitors: synthesis, crystal structure, molecular docking and DFT studies

Syeda Aaliya Shehzadi^{a,*}, Aamer Saeed^b, Fouzia Perveen^c, Pervaiz Ali Channar^b, Ifzan Arshad^{d,**}, Qamar Abbas^e, Saima Kalsoom^f, Sammer Yousaf^g, Jim Simpson^h^a Sulaiman Bin Abdullah Aba Al-Khail-Centre for Interdisciplinary Research in Basic Sciences (SA-CIRBS), International Islamic University, 44000 Islamabad, Pakistan^b Department of Chemistry, Quaid-i-Azam University, 45320 Islamabad, Pakistan^c Research Center for Modelling and Simulations (RCMS), National University of Sciences and Technology (NUST), H-12 Islamabad, Pakistan^d Department of Chemistry, University of Management and Technology, Sialkot, Pakistan^e Department of Physiology, University of Sindh, Jamshoro, Pakistan^f Department of Chemistry, Preston University, Islamabad, Pakistan^g H.E.J. Research Institute of Chemistry, International Center for Chemical and Biological Sciences, University of Karachi, 75270, Karachi, Pakistan^h Department of Chemistry, University of Otago, PO Box 56, Dunedin, New Zealand

GRAPHICAL ABSTRACT



ARTICLE INFO

Keywords:

N,S-heterocycles
 Thiazolidine-2-imines
 Crystal structures
 DFT studies
 Molecular docking
 Tyrosinase inhibitors

ABSTRACT

Various *N*- and *S*-containing 5-membered heterocycles such as imidazole-2-thiones, thiazolidinones and thiazolidin-2-imines are among the most eminent biologically active organic heterocycles and are present in many marketed drugs. In view of their synthetic and biological significance, an efficient synthesis of two novel thiazolidine-2-imines (**4a-b**) utilizing a three-component one-pot approach starting from an aldimine, an alkyne and isothiocyanates has been developed. The reaction proceeded via a 5-*exo digonal* (5-*exo dig*) cyclization of a propargyl thiourea, formed *in situ* in the presence of Zn^(II)-catalyst. The structures of the resulting products are elucidated by spectroscopic methods and X-ray crystallography. A DFT study explored the structural, thermodynamic and molecular electrostatic potential parameters for the compounds. The newly synthesized compounds (**4a** & **4b**) were evaluated for the inhibition of tyrosinase both *in vitro* and *in silico*. The *in vitro* results revealed that the synthesized thiazolidine-2-imines (**4a-b**) showed good inhibition activity towards mushroom tyrosinase (IC₅₀ = 1.151 ± 1.25 and 2.079 ± 0.87 μM respectively) in comparison to the kojic acid standard (IC₅₀ = 16.031 ± 1.27 μM) a commonly used anti-pigment agent in plant and animal tissues. The experimental inhibition was further

* Corresponding author.

** Corresponding author.

E-mail addresses: aaliya.shehzadi@iiu.edu.pk (S.A. Shehzadi), ifzan.arshad@skt.umt.edu.pk (I. Arshad).<https://doi.org/10.1016/j.heliyon.2022.e10098>

Received 11 May 2022; Received in revised form 6 July 2022; Accepted 26 July 2022

2405-8440/© 2022 The Author(s). Published by Elsevier Ltd. This is an open access article under the CC BY-NC-ND license (<http://creativecommons.org/licenses/by-nc-nd/4.0/>).

assessed by molecular docking studies between synthesized ligands and the human tyrosinase protein complex to investigate the intermolecular interactions responsible for tyrosinase inhibition activity.

1. Introduction

Melanin, which is responsible for the pigmentation of human skin, is produced in the melanocyte cells of the skin. Other than skin colour, dark coloured eyes, hair as well as browning of fruit and vegetables are also due to increased melanin content in the system. Production of melanin is catalysed by the enzyme tyrosinase in living organisms where the tyrosine is converted into dihydroxyphenyl alanine (DOPA), then to dopaquinone and finally to melanin [1, 2]. To reduce the content of melanin there is need to control the activity of tyrosinase. Therefore, the tyrosinase inhibitors are attractive in medicinal, cosmetic, food and agricultural industries as depigmentation or anti-browning agents. The cosmetic and food industries are always in search of less hazardous tyrosinase inhibitors for the treatment of skin conditions and for agricultural purposes [3, 4, 5, 6]. This has encouraged the scientists and researchers to focus on the synthesis, isolation, identification, and characterization of new active tyrosinase inhibitors [7, 8].

Various natural, semi-synthetic and synthetic inhibitors of tyrosinase with wide structural diversity have been developed [9] to date but very few advanced to the clinical phases as skin conditioning agents. Heterocycles have long and productive history in the pharmaceutical industry, where *N*- and *S*-containing 5 and 4-membered rings are among the more dominant motifs from synthetic and biological point of view [10, 11, 12, 13, 14]. Thiazoles, thiazolidinones and thiazolidin-2-imines are common structural units found in many natural products and pharmaceutically active molecules [15, 16, 17]. In addition, such structures also play important roles in the fields of organic and organometallic synthesis [18, 19, 20]. A few thiazolidine derivatives have been investigated for tyrosinase inhibition such as thiazolidinones substituted by hydrazone tautomeric dyes [21], thiazolidine-2,4-dione derivatives substituted with benzylidene [22], 2,4-dihydroxybenzylidene [23] 2, 4-dihydroxyphenylthiazolidine-4-carboxylic acid [22, 24, 25] and some iminothiazolidin-4-one derivatives [26]. Though a number of synthetic inhibitors showed inhibitory activity against mushroom tyrosinase, only a few of them displayed melanogenesis inhibition activity in human cells or skin models.

There has been a great deal of interest in the development of novel thiazolidine-2-imines in an effort to fine-tune the biological and physiological activities of such molecules. For the construction of the thiazolidin-2-imine ring several different synthetic routes have been adopted. The most prevalent is the reaction between propargyl amines and thiocyanates [27, 28, 29, 30]. In present study we have used a multicomponent approach to synthesize thiazolidine-2-imines so that their effectiveness as tyrosinase inhibitors could be examined. The process used starts from an aldimine, an alkyne and isothiocyanate as starting materials. This strategy avoids the need to make propargylamine separately in the synthetic process.

2. Results & discussions

2.1. Chemistry

To access the above thiazolidine-2-imines various catalysts and reaction conditions were investigated and optimized. Initially 2,2-dimethyl-*N*-propylpropan-1-imine (1), phenylacetylene (2) and 1-isothiocyanato-4-methylbenzene (3) were reacted together in toluene using CuCl₂ as a catalyst. A 35% yield of the expected thiazolidine, namely 5-benzylidene-4-(*tert*-butyl)-3-propyl-*N*-(*p*-tolyl)thiazolidin-2-imine (4a) was obtained (Table 1, entry 1). Switching to DMF as solvent increased the yield but replacing CuCl₂ with CuBr decreased the yield (Table 1, entries 2–3). The ZnI₂ proved to be more efficient than the Cu-

salts, preferably in DMF (Table 1, entries 4–5). Of the other Zn-salts such as Zn(OAc)₂, ZnCl₂ and ZnBr₂, zinc chloride was found to be the most efficient catalyst for the formation of expected thiazolidin-2-imine (4a) (Table 1, entries 6–8).

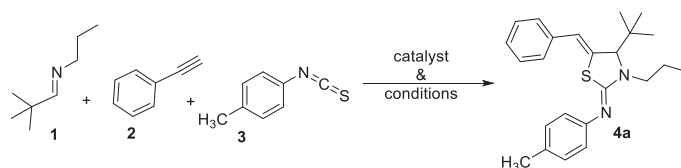
Using 20 mol % of zinc chloride while heating for 16 h at 100 °C proved to be the optimum condition of those examined for synthesizing target compounds 4a and 4b with 90 and 95 % yields respectively as shown in Scheme 1.

A plausible mechanism for the formation of thiazolidine-2-imine (4) is shown in Scheme 2. The reaction was anticipated as initial coupling of Zn-acetylide with aldimine 1 to give complex A, the nucleophilic attack of nitrogen of complex A on electrophilic carbon of isothiocyanate (3) yielded the intermediate propargyl thiourea (B) which after cyclization and basic treatment furnished the desired products (4a-b).

2.2. Structural analysis

Structural determinations of synthesized motifs were performed by spectroscopic (IR, Mass & NMR), single crystal x-ray analysis and DFT studies. The ¹H-NMR spectrum of compound 4a is shown in Figure 1. The methyl protons of *N*-propyl chain appeared as triplet at 0.92 ppm while nine protons of *tert*-butyl group appeared at 1.03 ppm as singlet. The *p*-methyl on phenyl ring appeared as singlet at 2.29 ppm. The two important signals which confirm the ring closure of propargyl thiourea are the one proton singlet at 4.05 ppm, which corresponds to the only proton of thiazolidine ring while other one proton singlet appeared at 6.47 ppm corresponds to 5-benzylidene proton. The ¹³C-NMR spectrum of compound 4a is shown in Figure 2, further confirmation of different quaternary carbons, CH, CH₂ and CH₃ groups were performed by ¹³C DEPT-135 NMR (Figure 3) and ¹³C APT-NMR (Figure 4) spectra. The quaternary carbon containing *tert*-butyl group which appeared at 39.4 ppm and two other quaternary carbons of phenyl rings which resonated at 149.0 and 157.6 ppm did not appear in the ¹³C DEPT-135 NMR spectrum while they clearly be seen in ¹³C APT-NMR spectrum in

Table 1. Optimization of imine 1, alkyne 2 and isothiocyanate 3 coupling under different reaction conditions.^[a]

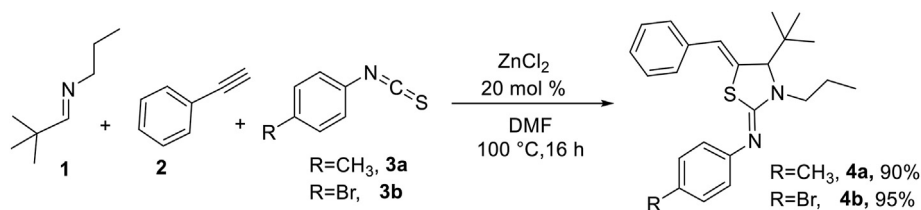


No	Catalyst (mol %)	Temp. (°C)	Time (h)	Solvent	Yield 4a (%) ^[b]
1	CuCl ₂ (20)	60	10	toluene	35
2	CuCl ₂ (20)	100	10	DMF	45
3	CuBr (20)	100	10	DMF	20
4	ZnI ₂ (20)	60	10	DMF	68
5	ZnI ₂ (20)	60	10	toluene	50
6	Zn(OAc) ₂ (20)	60	10	DMF	NR ^[c]
7	ZnCl ₂ (10)	60	16	DMF	70
8	ZnBr ₂ (15)	60	18	DMF	59
9	ZnCl ₂ (15)	100	10	DMF	80
10	ZnCl ₂ (20)	100	16	DMF	90

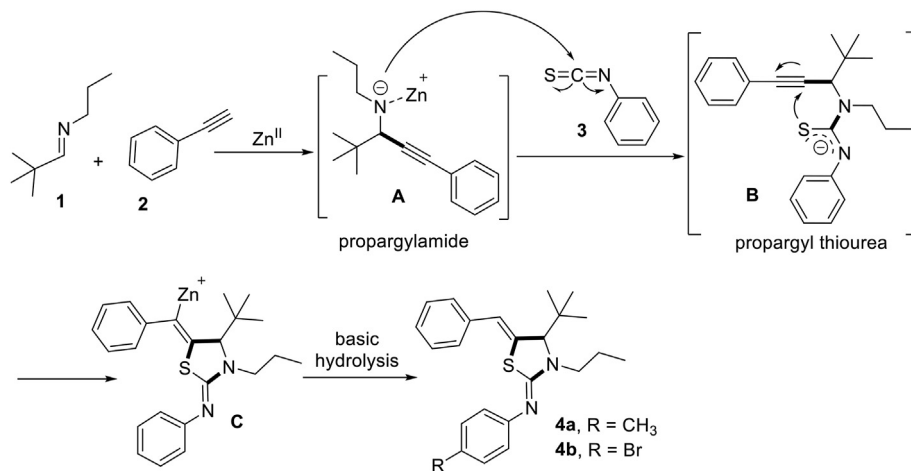
^[a]All reactions were performed on 1.0 mmol scale of aldimine 1.

^[b]¹H-NMR yield.

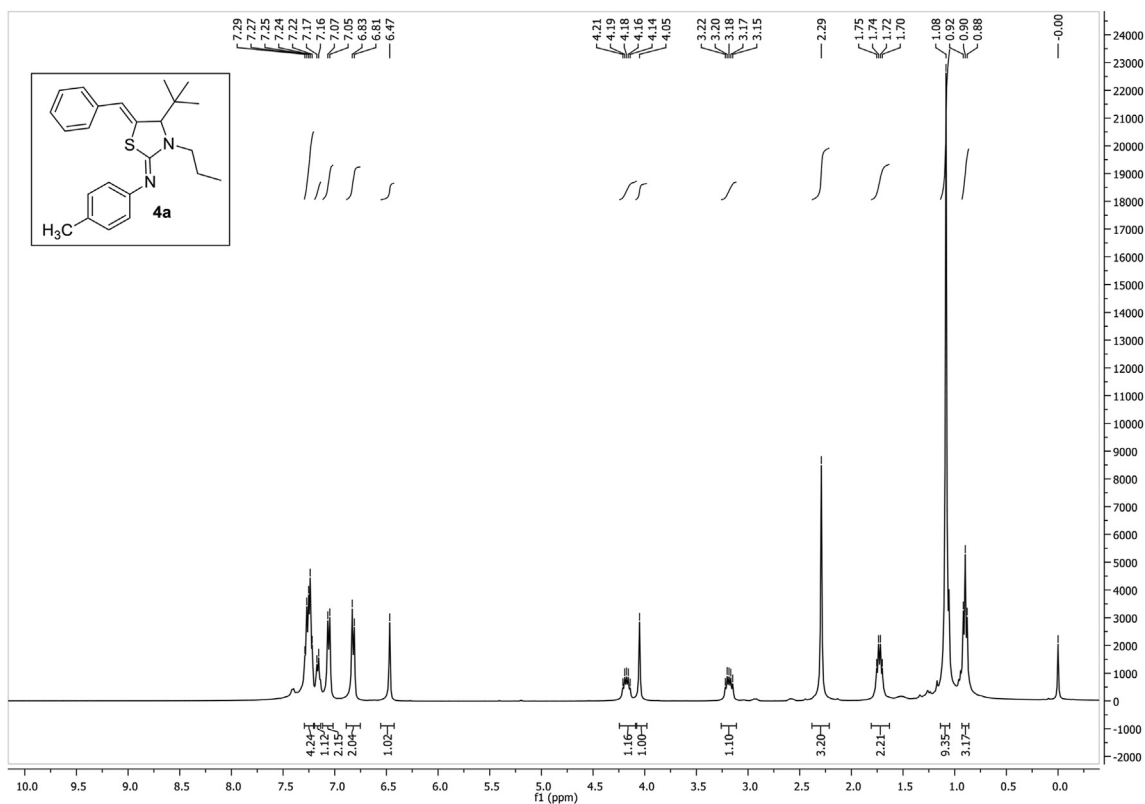
^[c]No Reaction.



Scheme 1. Synthesis of targeted thiazolidine-2-imines (4a-b).



Scheme 2. Proposed mechanism for the formation of thiazolidine-2-imines (4).

Figure 1. ¹H-NMR (400 MHz) spectrum of 4a in CDCl₃.

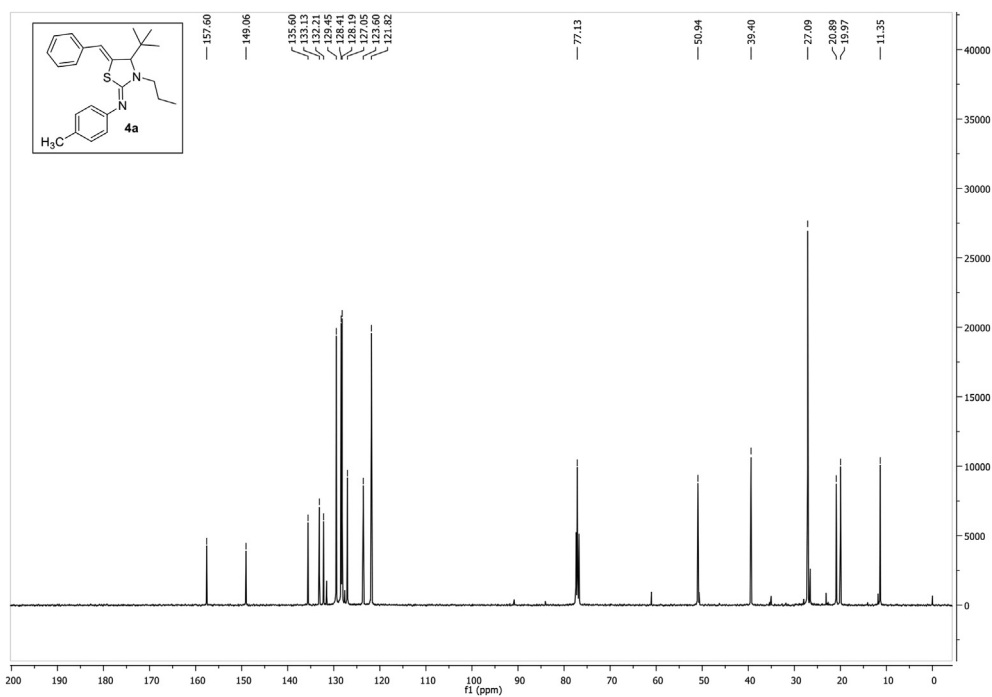


Figure 2. ^{13}C -NMR (100 MHz) spectrum of **4a** in CDCl_3 .

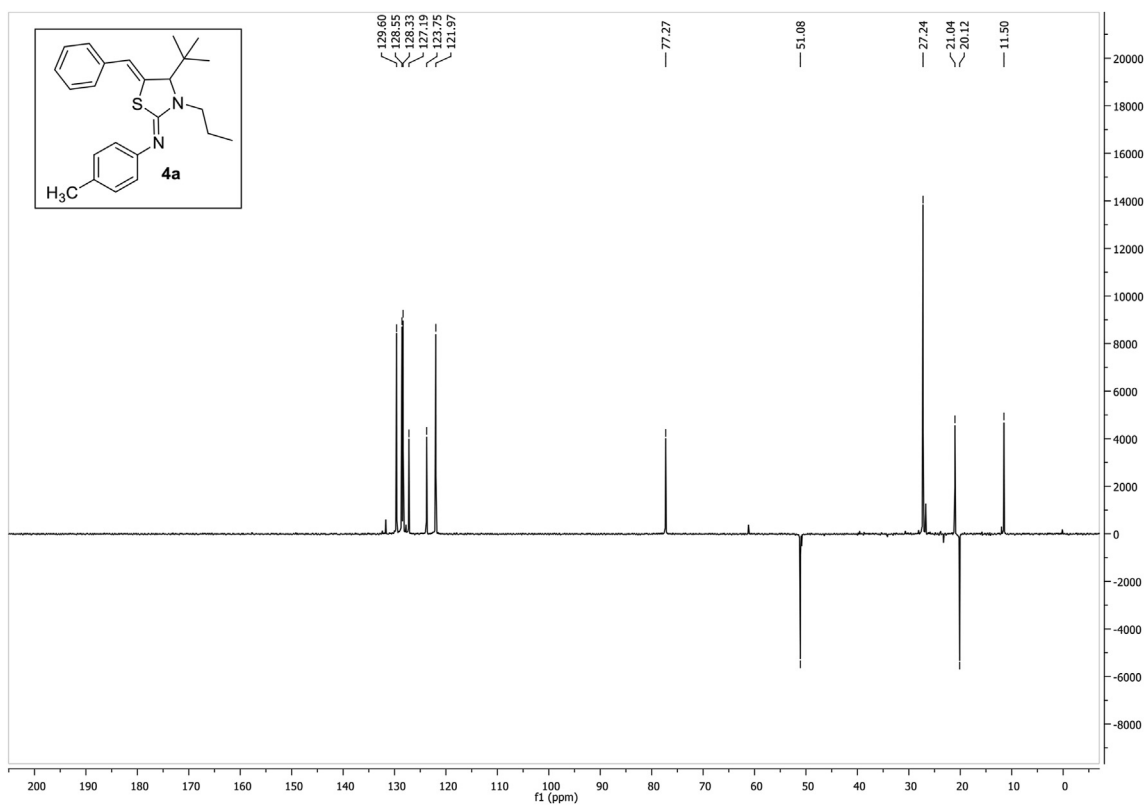


Figure 3. ^{13}C DEPT-135 NMR (100 MHz) spectrum of **4a** in CDCl_3 .

negative region. The ^1H -NMR and ^{13}C -NMR spectra of compound **4b** are shown in Figure 5 and Figure 6 respectively. The chemical shift values have been shifted little bit downfield due to presence of electron withdrawing 4-bromo group.

2.2.1. Molecular structure

The molecular structures of **4a** and **4b** are sufficiently similar except for substitution of methyl and bromo group at phenyl ring and the structure of **4a** is shown in Figure 7. In the compound **4a** an

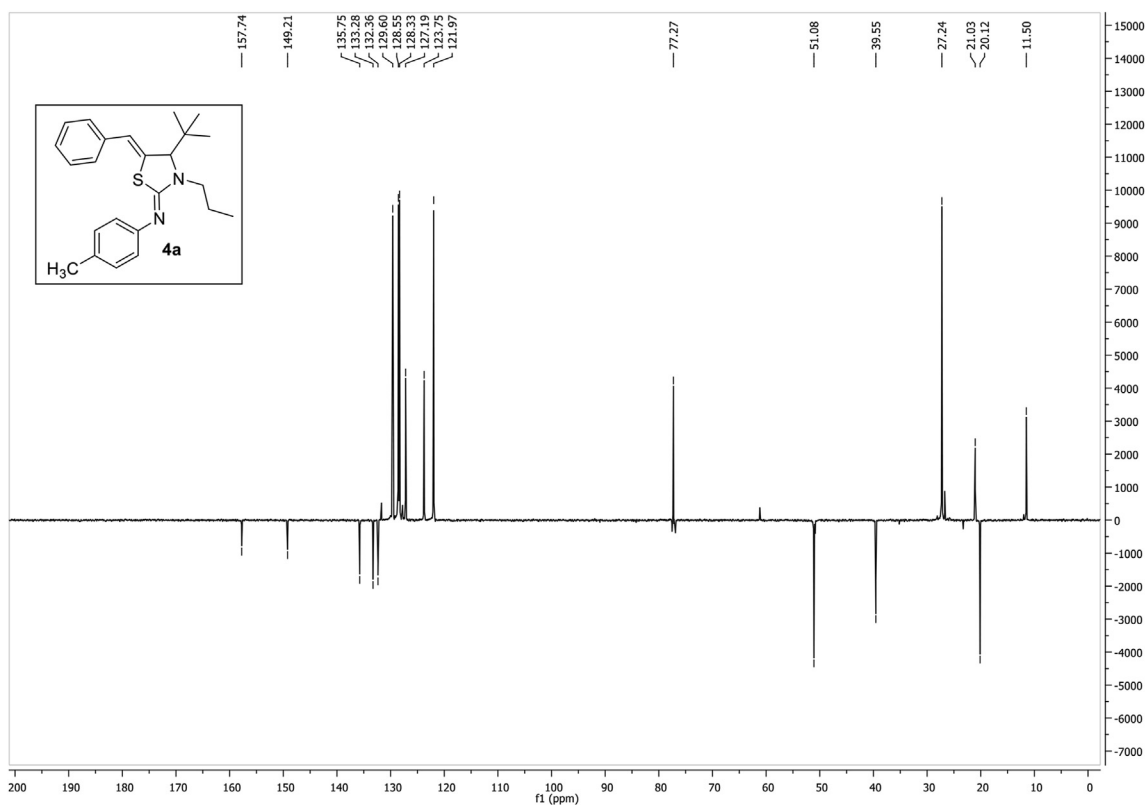


Figure 4. ^{13}C APT-NMR (100 MHz) spectrum of **4a** in CDCl_3 .

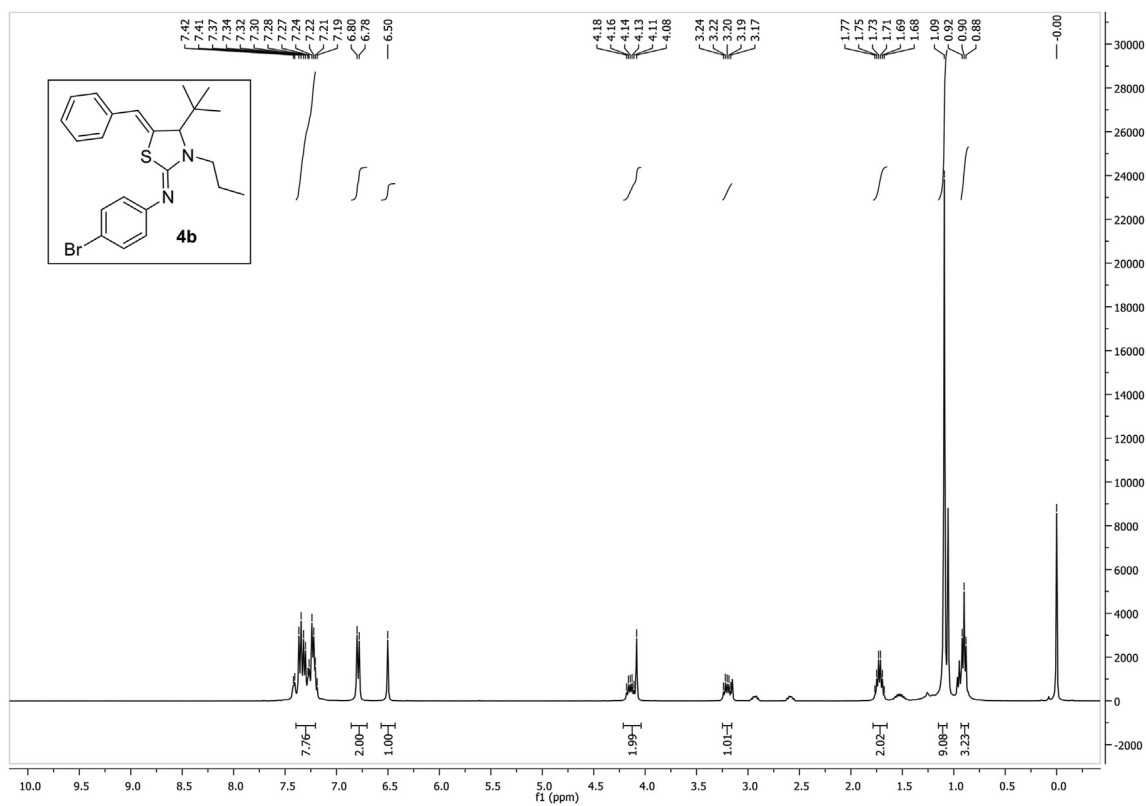


Figure 5. ^1H -NMR (400 MHz) spectrum of **4b** in CDCl_3 .

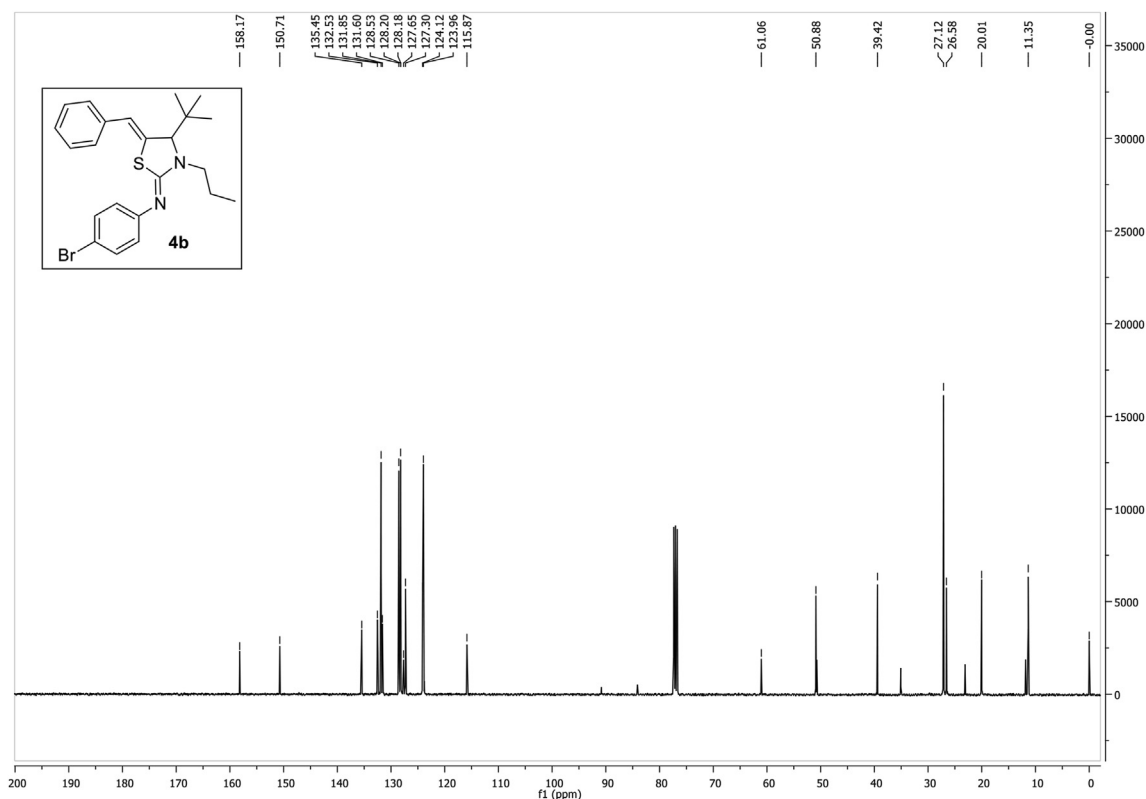


Figure 6. ^{13}C -NMR (100 MHz) spectrum of **4b** in CDCl_3 .

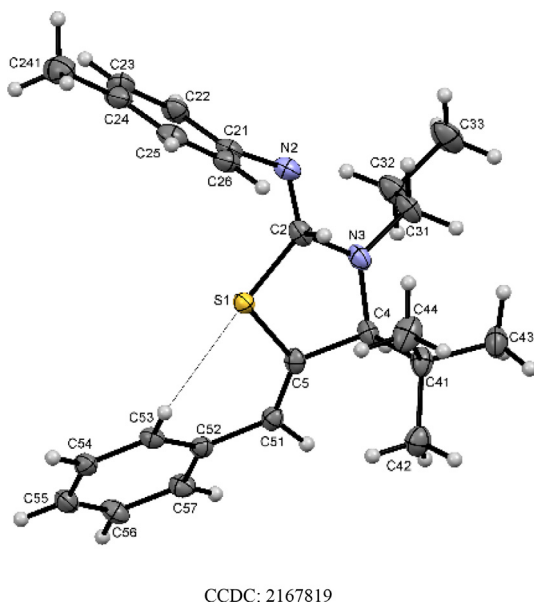


Figure 7. The molecular structures of **4a** with ellipsoids drawn at the 50% probability level. Intramolecular hydrogen bonds are drawn as black dotted lines.

intramolecular C53–H53...S1 hydrogen bond (Table 3), links the S atom of the thiazolidine rings to the phenyl ring of the benzylidene substituent enclosing S(6) ring [31]. The thiazolidine ring adopt envelope conformation on C5. The molecule is not planar with the thiazolidine ring of **4a** inclined to the *p*-tolyl and phenyl rings by 76.85(6)° and 50.04(7)°. The additional propyl- and *t*-butyl substituents on the 3- and 4-positions of the thiazolidine ring of molecule lead to crowded environment both above and below the thiazolidine ring planes.

Table 2. Percentage individual contributions of interatomic contacts to the Hirshfeld surfaces of **4a** and **4b**.

#	Contact	4a %	4b %
1	H...H	70.7	56.1
2	H...C/C...H	23.6	24.9
4	H...S/S...H	3.3	3.2
5	H...N/N...H	2.4	2.6
3	H...Br/Br...H		12.9
6	Br...S		0.2
7	Br...Br		0.1

Table 3. Optimized geometrical parameters of **4a** using B₃LYP/6-31G(d,p) level.

Bond lengths (Å ^o)		Bond angles (°)	
S(14)–C(12)	1.831	S(14)–C(12)–C(13)	109.94
N(13)–C(16)	1.266	C(13)–N(15)–C(16)	118.76
C(16)–N(15)	1.369	N(15)–C(16)–N(30)	124.38
C(14)–N(15)	1.458	C(16)–N(30)–C(34)	129.57
C(31)–C(35)	1.512	N(15)–C(41)–C(42)	112.02
C(2)–C(3)	1.402	S(14)–C(12)–C(51)	126.56
C(5)–H(10)	1.081	C(4)–C(2)–C(3)	112.97
C(41)–N(15)	1.481	N(30)–C(34)–C(33)	117.58
C(22)–C(17)	1.545	C(13)–C(17)–C(22)	109.02

2.2.2. Crystal packing

In the packing of **4a** molecule, C51–H51...N2 hydrogen bonds, Table 2, link molecule into C(6) chains along the *a* axis direction shown in Figure 8. These unusual coincidences continue as these C–H...N hydrogen bonds combine with C55–H55...Cg2 contacts (Cg2 is the

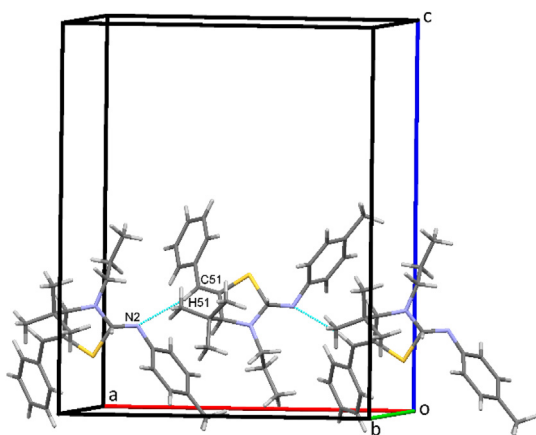


Figure 8. Chains of molecules of 4a along the a axis direction.

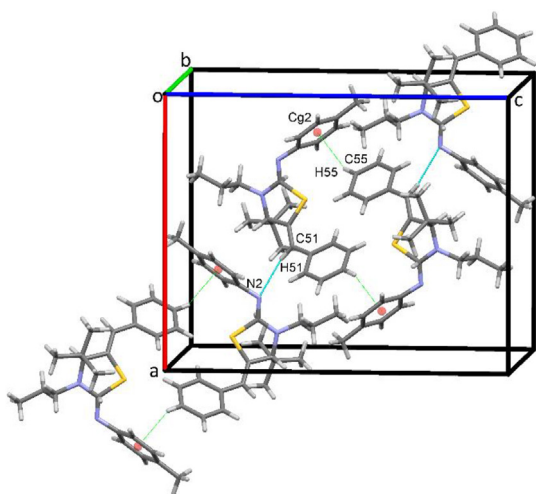


Figure 9. Double chains of molecules of 4a along the ac diagonal.

centroid of the C21...C26 benzene ring) to form double chains of molecules along the ac diagonal of each unit cell [Figure 9](#).

2.2.3. Hirshfeld surface analysis

Hirshfeld surface analysis [[32](#)] can be used to further investigate and compare the intermolecular architecture of these molecules. Hirshfeld

surfaces and two-dimensional fingerprint plots were generated by *CrystalExplorer* (Turner et al., *CrystalExplorer17*, 2017) as shown in [Table 2](#).

Hirshfeld surface analysis can be used to further investigate and compare the intermolecular architecture of these molecules. Hirshfeld surfaces viewed for front (a) and rear (b) faces of **4a** and for **4b** are shown in [Figures 10](#) and [11](#) respectively. The deep red circles on [Figure 10\(a\)](#) and [11\(a\)](#) surfaces correspond to the C51–H51...N2 hydrogen bonds that are present in both molecules, and the weaker C–H...O hydrogen bond and the Cl... π (ring) halogen bond. As indicated previously, these contacts play considerable roles in stabilizing the packing in this structure.

Hirshfeld surfaces and two-dimensional fingerprint plots were generated by *CrystalExplorer* (Turner et al., *CrystalExplorer17*, 2017). Fingerprint plots of the principal contacts on the Hirshfeld surface of **4a** and **4b** are shown in [Figure 12a](#) and b. These comprise H...H, H...C/C...H, H...S/S...H, H...N/N...H contacts and an additional substantial H...Br/Br...H contact for **4b**, [Figure 7k](#). The much less significant Br...S and Br...Br contacts, that together contribute only 0.5% to the Hirshfeld surface, are not shown in the figure but the completeness is detailed in [Table 2](#).

3. Theoretical structural analysis

Structural geometries of compounds **4a** and **4b** were simulated and optimized using DFT/B3LYP to determine geometric and electronic parameters (bond lengths, bond angles, E_{HOMO} , E_{LUMO}). The optimized geometries of **4a**, **4b** are shown in [Figure 13](#), while important geometric parameters (bond lengths and bond angles) are summarized in [Tables 3](#) and [4](#).

3.1. Absorption studies and frontier molecular orbitals (FMOs) analysis

Simulated absorption spectra for compounds **4a** and **4b** were obtained from a time dependent calculation using B3LYP/6-31G(d,p) level of theory. Theoretically calculated absorption spectra showed absorption peaks at 325 nm and 687 nm for **4a** ([Figure 14a](#)). The corresponding values for **4b** exhibited absorption maxima at 318 nm and 694 nm ([Figure 14b](#)). Absorption maxima for both compounds result from π - π^* electronic transitions.

The frontier molecular orbital (FMOs) analysis carried out using a quantum mechanical approach is a popular way to predict the molecular transitions [[33](#), [34](#)]. The corresponding E_{HOMO} and E_{LUMO} values were -7.18eV and -4.77eV for compound **4a** with band gap of 2.14eV ([Figure 15A](#)). The E_{HOMO} , E_{LUMO} and band gap values for **4b** were found to be -6.24eV, -5.06 eV and 1.18 eV respectively ([Figure 15B](#)). To comprehend the distribution of isodensities of HOMO and LUMO surfaces, it can be observed that isodensities are distributed on heteroatom.

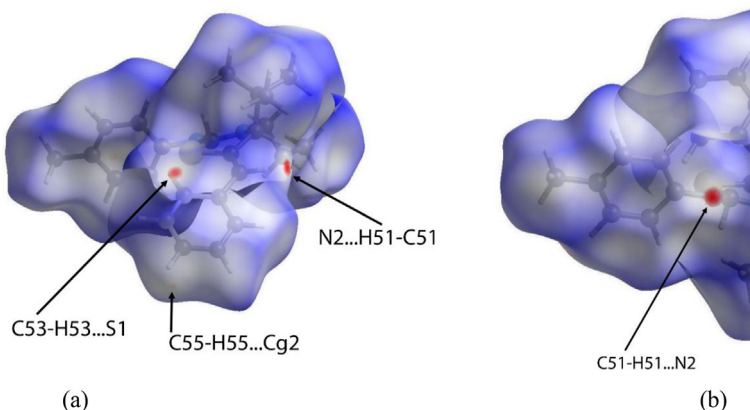


Figure 10. Hirshfeld surfaces mapped over d_{norm} showing front (a) and rear (b) faces of molecule 4a.

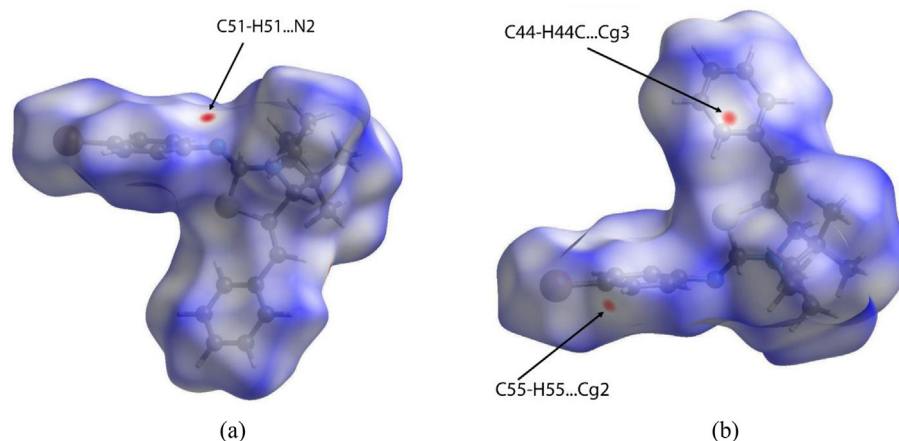


Figure 11. Hirshfeld surfaces mapped over d_{norm} showing front (a) and rear (b) faces of molecule 4b.

3.2. Thermodynamic parameters

Based on vibrational analysis using frequency calculations and statistical thermodynamics, a number of thermodynamic parameters i.e; heat capacity (C_v), entropy (S_0) and enthalpy (H^0) were calculated and listed in Table 5. Zero point vibrational energies have also been calculated for accurate description of structure. The variations in the entropy and zero-point vibrational energies were found to be insignificant.

3.3. Molecular electrostatic potential analysis

Optimized geometries at B3LYP/6-31G(d,p) level of theory were used to map the molecular electrostatic potential surfaces (MESP) of compounds 4a and 4b and are shown in Figure 16. It is evident from Figure 11 that negative potential is concentrated on oxygen, sulfur and bromine atoms which reflects electron transfer from O, S and Br. The dispersion of potential for 4a ranges from -0.01225 to 0.01225 esu and from -0.00885 to 0.00885 esu for 4b.

4. Biological evaluation

Both compounds were tested for their inhibition activity against the mushroom tyrosinase enzyme using a previously reported procedure [35, 36, 37, 38, 39]. The results are summarized in Table 6.

Both compounds were found to be more active than the Kojic acid, which was used as a standard. The compound 4a was even more active than 4b perhaps because of the presence of a CH_3 substituent at para position of the benzene ring.

5. Molecular docking and computational analysis for tyrosinase inhibition

Molecular docking analysis was carried out in order to understand the binding mode of synthetic thiazolidin-2-imines in active site of tyrosinase. Molecular Operating Environment software 2016.0802 was used for molecular modelling studies. MOE is a software system designed by a Chemical Computing Group to support cheminformatics, bioinformatics, molecular modelling, virtual Screening, structure and ligand based-design (Scientific Vector Language). As most tyrosinase inhibitors have been tested with commercial mushroom tyrosinase for use against mammalian tyrosinases therefore to understand the

inhibitory activity of both compounds at the molecular level, docking studies were performed using the active site of the human tyrosinase protein complex (PDB ID: 2XV7) obtained from the Protein Databank (PTB). Figure 17 depicts the active site of tyrosinase complex with co-crystallized ligand neuregulin (NRG). Key contributing amino acids in this site are Leu124, Tyr 160, Glu123, Arg141, Thr158, His186, Lys182, Ala184 and Val183.

Since Kojic acid has higher *in vitro* inhibitory activity on human tyrosinase and has been clinically used to treat the hyperpigmentation of skin, first the molecular interactions of Kojic acid were explored in the active site of tyrosinase. The results revealed that two Hydroxyl groups of kojic acid have hydrogen bonding with three amino acids Lys182, Val120 and Glu123 with distance 1.77 \AA , 2.37 \AA and 3.68 \AA respectively as shown in Figure 18. Docked binding score for this complex is -9.88 kcal/mol .

Finally, the molecular docking study of synthesized ligands (4a & 4b) was performed. Ten different conformations were generated for each molecule and lowest energy conformation was selected for binding interactions analysis as shown in Figure 19.

In silico studies revealed that both compounds were fitted well in the active site of the targeted protein. The high activity of both compounds may be due to presence of an aromatic ring and more hydrophobic centres giving rise to the arene- π and hydrophobic interactions respectively. Both compounds have strong hydrogen bonding and arene- π interactions with key contributing amino acids as shown in Figures 20 and 21. The compound 4a has an arene- π interaction with Phe140, a π - π interaction with His186 and hydrogen bonding interactions with Arg141 (Figure 20). While compound 4b has an arene- π interaction with Arg141 and hydrogen bonding interactions with both Glu123 and Thr130 (Figure 21). The docked binding score for compound 4a is -11.51 kcal/mol and for 4b is -13.23 kcal/mol Table 7 summarises all important intermolecular interactions and key amino acids that might be responsible for the high inhibition activity of both compounds suggesting that such thiazolidine-2-imines (4a-b) could be potent candidates for anti-browning agents.

6. Conclusion

In summary two novel thiazolidine-2-imines (4a-4b) have been synthesized in good yield starting from imine, alkyne and isothiocyanate using Zn^{II} -catalysis. The structural and molecular characterization

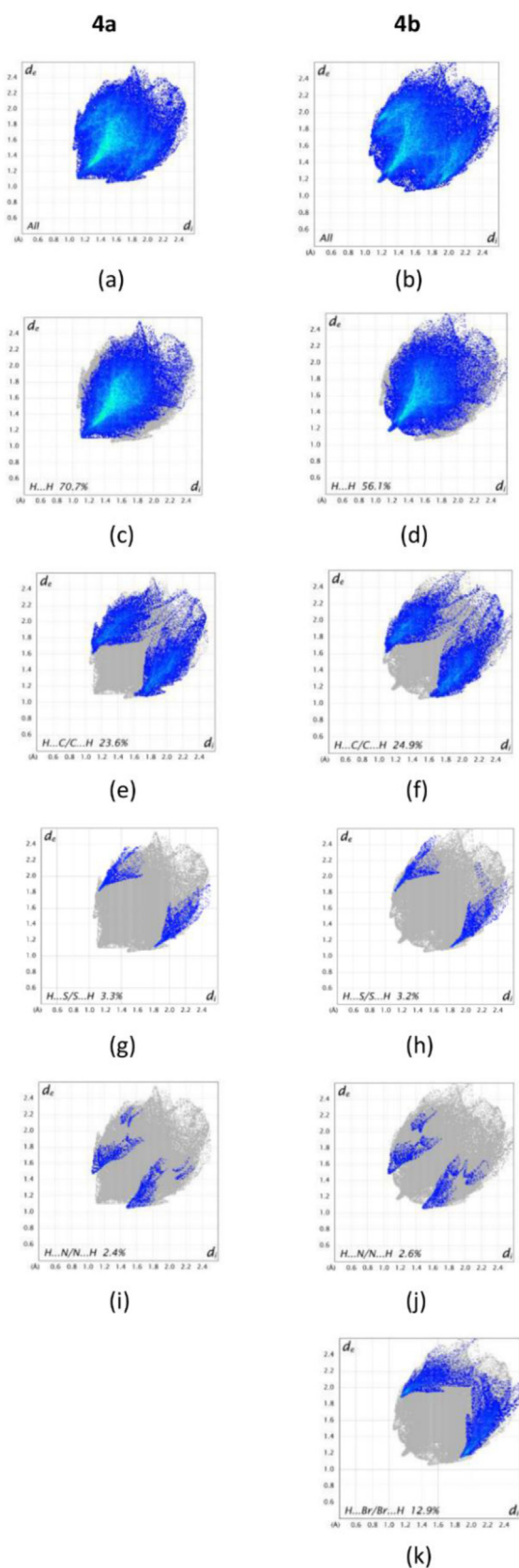


Figure 12. Full two-dimensional fingerprint plot for **4a** (a) and **4b** (b), while (c)–(k) are the principal individual contact types for **4a** on the left and **4b** on the right.

has been accomplished by spectroscopic, single crystal X-ray analysis and DFT studies. A detailed Hirshfeld surface analysis was carried out for the exploration and picturing of the intermolecular close contacts in the crystal structure of the synthesized compounds, and also to investigate the locations of atom...atom short contacts with potential to form hydrogen bonds and the quantitative ratios of these interactions. Quantum DFT for structural and parametric analyses indicated that compounds **4a** and **4b** are reactive. Both compounds were found to be excellent inhibitors when tested against a mushroom tyrosinase inhibition assay with IC_{50} value of 1.151 ± 1.25 and 2.079 ± 0.87 compare to the Kojic acid as standard drug (16.03 ± 1.27). Further molecular docking studies of synthesized compounds with human tyrosinase protein (PDB id: 2XV7) using MOE software revealed that these ligands fit into the active site of target protein with the major contacts including hydrogen bonding, arene-arene and arene- π interactions. The excellent agreement was obtained between the molecular modelling and the tyrosinase inhibition assay which indicated that the binding mode proposed is reasonably close to the experimental biological binding modes. This study should therefore prove helpful for further optimization in *in-vitro* and animal models before clinical trials.

7. Experimental

7.1. General remarks and instrumentation

All the chemicals and solvents of analytical grade were purchased from commercial sources and were used as such without further purification. The reactions were performed under normal atmospheric conditions. The melting points were recorded on electrothermal 1101D Mel-Temp digital melting point apparatus. 1H -NMR and ^{13}C -NMR spectra were recorded on 400 MHz and 100 MHz Bruker spectrometer respectively in deuterated solvent containing TMS as internal standard. Chemical shift values are given in part per million (ppm). High-resolution mass spectra were obtained on an Agilent 6210 TOF LC/MS mass spectrometer.

7.2. Experimental procedure for the synthesis of the thiazolidin-2-imines (**4a-b**)

To a magnetically stirred solution of aldimine **1** (2.00 mmol), phenylacetylene **2** (2.00 mmol) and isothiocyanate **3** (2.00 mmol) in dry DMF, zinc(II) chloride (0.20 mmol, 20 mol %) was added. The flask was attached with a condenser and covered with a N_2 balloon. The mixture was heated at $100^\circ C$ for 16 h. Afterwards, the mixture was cooled, washed with a dilute solution of $NaHCO_3$ and extracted with EtOAc. The combined organic layers were dried using anhydrous Na_2SO_4 , filtered and the solvent was evaporated under reduced pressure. Final products were purified by column chromatography using petroleum ether/EtOAc (85:15) as the solvent system.

7.2.1. 5-(Benzylidene)-4-(tert-butyl)-3-propyl-N-(p-tolyl)thiazolidin-2-imine (**4a**)

Light-yellow block crystals; m.p = $78^\circ C$, 80% yield. 1H NMR (400 MHz, $CDCl_3$) δ = 7.33 – 7.14 (m, 5H, Ar), 7.06 (t, J = 7.4 Hz, 2H, Ar), 6.82 (d, J = 7.4 Hz, 2H, Ar), 6.47 (s, 1H, $\underline{H}C = CS$), 4.18 (dt, J = 14.2, 7.2 Hz, 1H, \underline{NCHH}), 4.05 (s, 1H, $\underline{H}CC(CH_3)_3$), 3.18 (dt, J = 14.2, 7.2 Hz, 1H, \underline{NCHH}), 2.29 (s, 3H, \underline{CH}_3Ph), 1.79 – 1.70 (m, 2H, $\underline{NCH}_2\underline{CH}_2$), 1.08 (s, 9H, $\underline{C(CH}_3)_3$), 0.90 (t, J = 7.4 Hz, 3H, $\underline{CH}_2\underline{CH}_3$). ^{13}C NMR (100 MHz, $CDCl_3$) δ = 157.60, 149.06, 135.60, 133.13, 132.21, 129.45, 128.41, 128.19, 127.05, 123.60, 121.82, 77.13, 50.94, 39.40, 27.09, 20.89, 19.97, 11.35. HRMS (ESI): m/z calcd for $[C_{24}H_{30}N_2S + H]^+$: 379.2202; found 379.2204.

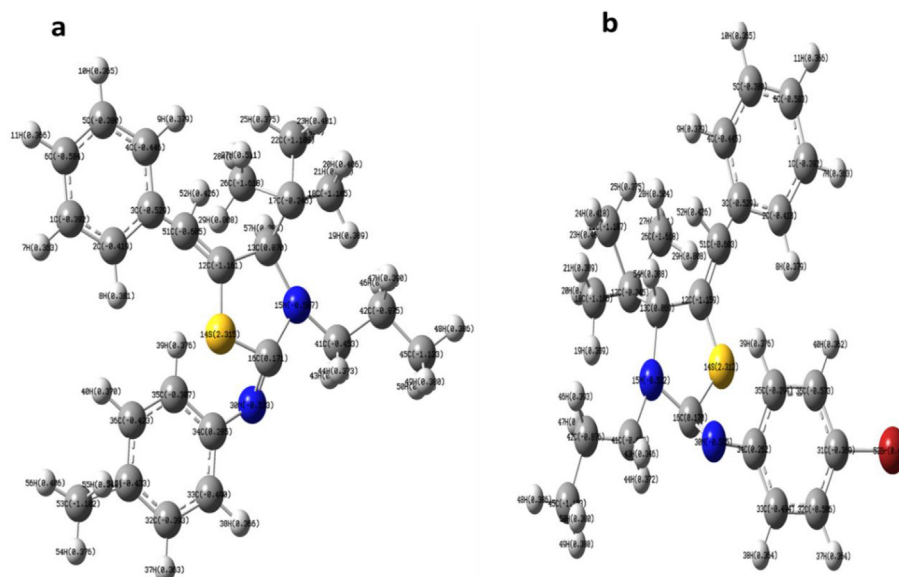


Figure 13. The optimized geometry of compounds (4a,4b) at the B₃LYP/6-31G (d,p) level of theory.

Table 4. Optimized geometrical parameters of 4b using B₃LYP/6-31G(d,p) level.

Bond lengths (Å ^b)		Bond angles (° ^b)	
S(14)–C(12)	1.833	Br(53)–C(31)–C(32)	119.26
C(16)–N(15)	1.373	C(34)–N(30)–C(16)	128.54
N(30)–C(16)	1.277	N(30)–C(16)–N(15)	124.06
N(30)–C(34)	1.422	N(15)–C(13)–C(12)	106.19
C(41)–N(15)	1.471	S(14)–C(12)–C(13)	109.76
C(13)–N(15)	1.472	S(14)–C(12)–C(13)	126.03
C(41)–N(42)	1.531	N(15)–C(41)–C(42)	112.87
Br(53)–C(31)	1.921	C(26)–C(17)–C(18)	108.13
C(17)–C(26)	1.541	C(51)–C(3)–C(4)	117.14

7.2.2. 5-(Benzylidene)-N-(4-bromophenyl)-4-(tert-butyl)-3-propylthiazolidin-2-imine (4b)

Viscous oil which became crystalline solid on standing and it was recrystallized in ethyl acetate; m.p = 80 °C, 89% yield. ¹H NMR (400 MHz, CDCl₃) δ = 7.43 – 7.19 (m, 7H, Ar), 6.79 (d, *J* = 8.4 Hz, 2H, Ar), 6.50 (s, 1H, HC = CS), 4.14 (dt, *J* = 14.2, 7.2 Hz, 1H, NCHH), 4.08 (s, 1H, HCC(CH₃)₃), 3.20 (dt, *J* = 14.2, 7.2 Hz, 1H, NCHH), 1.77 – 1.68 (m, 2H,

CH₂CH₃), 1.09 (s, 9H, C(CH₃)₃), 0.90 (t, *J* = 7.4 Hz, 3H, CH₂CH₃). ¹³C NMR (100 MHz, CDCl₃) δ = 158.17, 150.71, 135.45, 132.53, 131.85, 131.60, 128.53, 128.20, 128.18, 127.65, 127.30, 124.12, 123.96, 115.87, 61.06, 50.88, 39.42, 27.12, 26.58, 20.01, 11.35. HRMS (ESI): *m/z* calcd for [C₂₃H₂₇BrN₂S + H]⁺: 443.1151; found 443.1146.

7.3. X-ray structure determination

Crystallographic data for compounds 4a is listed in Table 8. Diffraction data were collected on an Agilent Duo diffractometer using Cu- α radiation (λ = 1.5417 Å). Data collection, reduction and absorption corrections for both were controlled using CrysAlisPro with data collected at 273(2) K. The structures were all solved with SHELXTL [40] and refined by full-matrix least-squares on F² using SHELXL-2016 [41] and TITAN2000. All non-hydrogen atoms were assigned anisotropic displacement parameters. All H-atoms were positioned geometrically and refined using a riding model with d(C–H) = 1.00 Å for methine, 0.99 Å for methylene, and 0.95 Å for the aromatic hydrogen atoms with U_{eq} = 1.2U_{eq}(C). Methyl protons had d(C–H) = 0.98 Å with U_{eq} = 1.5U_{eq}(C). All molecular plots and packing diagrams were drawn using Mercury [42]. Other calculations were performed using PLATON [43] and tabular material was produced using WINGX [44].

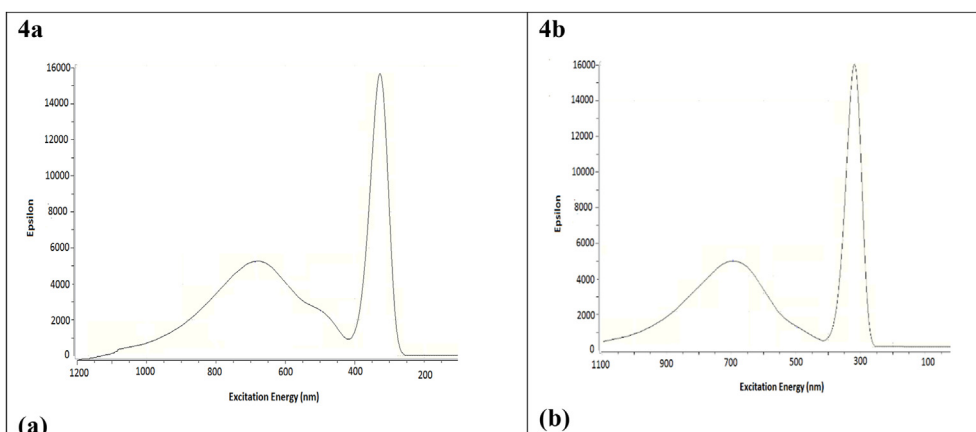


Figure 14. Theoretically Simulated UV-Vis spectra of compound 4a (a) and of compound 4b (b).

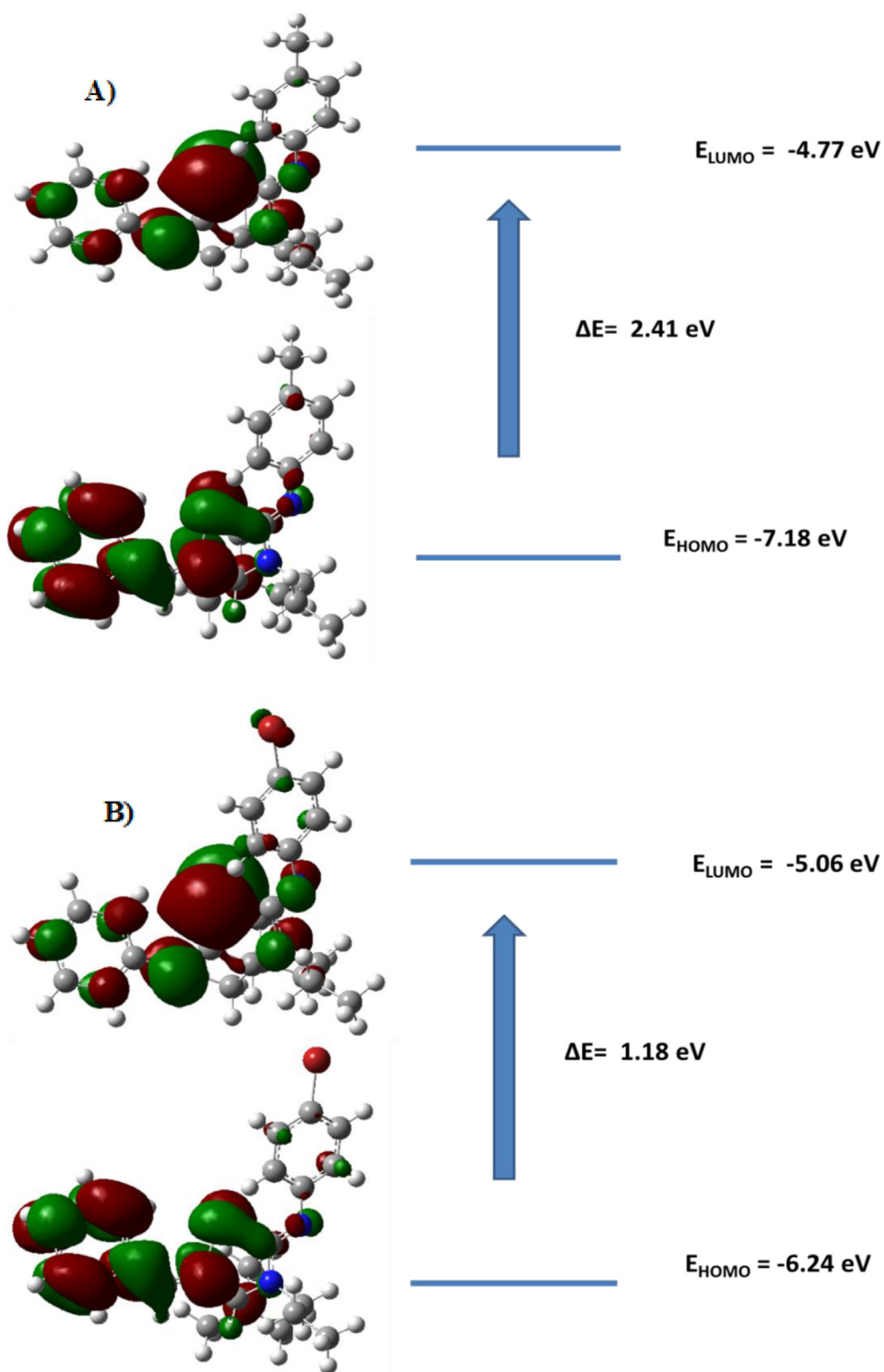


Figure 15. HOMO, LUMO, E_{HOMO} , E_{LUMO} and band gap (ΔE) for compound 4a (A) and 4b (B).

Table 5. Calculated thermodynamic parameters of synthesized compounds (4a-b).

Parameters	4a	4b
Total Thermal E (kcal/mol)	318.638	295.24
Heat Capacity (C _v)/Cal/Mol-K	69.196	68.951
Entropy (S ⁰) (Cal/Mol/K)	127.531	130.313
Enthalpy (Kcal/mol)	-3913.105437	-3952.105437
Free Energy (Kcal/mol)	-3913.12421	-3952.167353
Zero-point vibrational energy (Kcal/Mol)	308.68476	285.04516
Dipole Moment (D)	2.5792	0.5278

7.4. Quantum Chemical studies

Quantum Chemical studies were carried out using Gaussian 09 software, [45] Gauss view 05 was employed for graphics visualization, compounds **4a** and **4b** had been optimized at hybrid B3LYP method with 6-31G(d,p) basis set. Geometry confirmation of **4a** and **4b** was explored through frequency analysis at the same level of theory, and no imaginary frequencies were observed (true minima). Theoretical vibrational analysis and thermodynamic analysis was also performed using frequency calculations. DFT calculations of the absorption spectra were executed at B3LYP/6-31G(d,p) level of theory. A total of 6 excited states (3 singlet and 3 triplet) were considered for the computation of the UV-Vis spectra of compound **4a** and **4b**. Frontier molecular orbitals, molecular electrostatic potential (MEP) and band gaps were also calculated at the B3LYP/6-31G(d,p) level of theory.

7.5. Mushroom tyrosinase inhibition assay (IC₅₀)

The mushroom tyrosinase (Sigma Chemical, USA) inhibition assay was performed following our previously reported methods [35, 36, 37, 39] with L-DOPA as substrate and kojic acid as reference inhibitor. In detail, 140 μL of phosphate buffer (20 mM, pH 6.8), 20 μL of mushroom tyrosinase (30 U/mL) and 20 μL of the inhibitor solution were placed in the wells of a 96-well micro plate. After pre-incubation for 10 min at room temperature, 20 μL of L-DOPA (3,4-dihydroxyphenylalanine, Sigma Chemical, USA) (0.85 mM) was added and the assay plate was further incubated at 25 °C for 20 min. Afterward the absorbance of dopachrome was measured at 475 nm using a micro plate reader (OPTI Max, Tunable). Kojic acid was used as a reference inhibitor and phosphate buffer was used as a negative control. The amount of inhibition by the test

Table 6. The inhibitory effects of 4a-b on mushroom tyrosinase activity.

Compound	Tyrosinase inhibition activity IC ₅₀ ± SEM (μM)
4a	1.151 ± 1.25
4b	2.079 ± 0.87
Kojic acid	16.031 ± 1.27

SEM = Standard error of the mean; values are expressed in mean ± SEM.

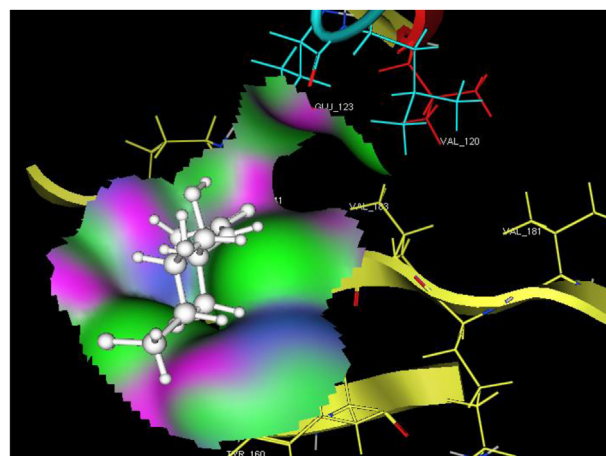


Figure 17. The active site of the tyrosinase protein complex PDB 2XV7 with neuregulin (NRG) co-crystallized inside it. The green areas show hydrophobic regions, while the purple area show hydrophilic areas.

compounds was expressed as the percentage of concentration necessary to achieve 50% inhibition (IC₅₀).

Each concentration (0, 20, 40, 60, 80, 100 μM) synthesized compounds dissolved in DMSO, final concentration 7% v/v) were firstly prepared and analysed in three independent experiments. The IC₅₀ values were determined by the data analysis and graphing software Origin 8.6, 64-bit.

The % of Inhibition of tyrosinase was calculated as following equation

$$\text{Inhibition (\%)} = [(B-S)/B] \times 100$$

Here, the B and S are the absorbances for the blank and for the samples.

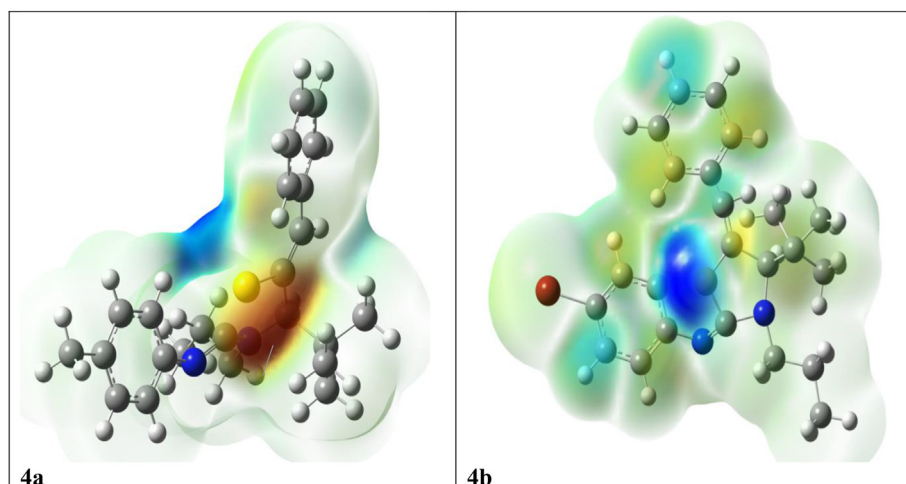
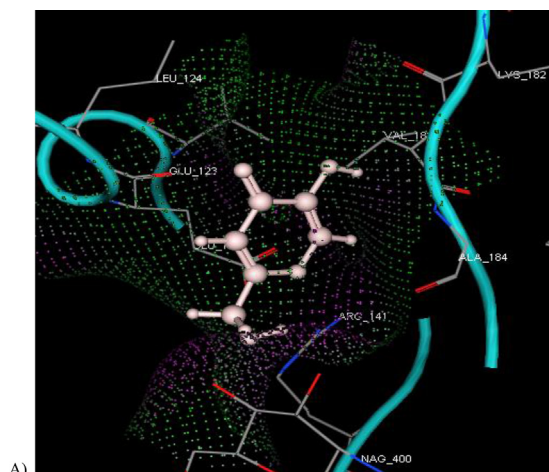
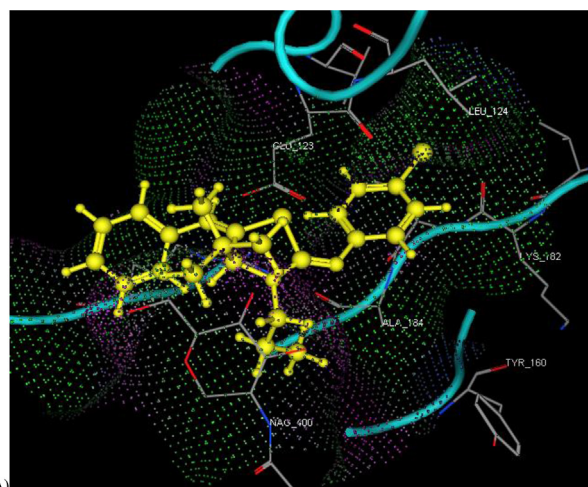


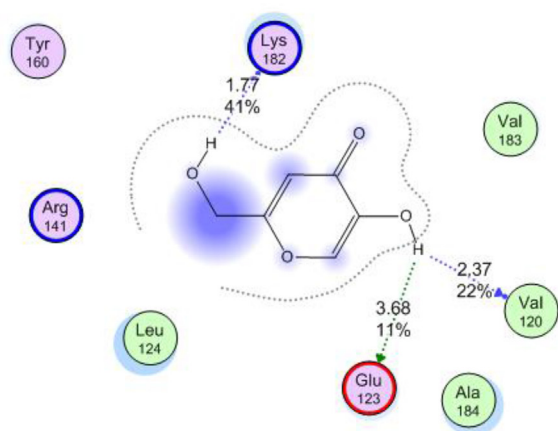
Figure 16. Molecular electrostatic potential surfaces (MESP) of compounds **4a** and **4b**.



A)



A)



B)

Figure 18. The 3D (A) & 2D (B) docked view of Kojic acid in the active site of tyrosinase complex.

7.6. Materials & methods for molecular docking

The molecular docking tool, MOE 2018 was used for ligand docking studies into the Tyrosinase binding pocket. The crystal structure of target was obtained from the protein data bank (PDB ID: 2XV7). The structures of compounds were prepared using the builder tool of MOE. The energy of the protein molecule was minimized using the Energy minimization algorithm of the MOE tool. The following parameters were used for energy minimization;

Gradient: 0.05,
Force Field: MMFF94X + Solvation,
Chiral Constraint: Current Geometry.

Energy minimization was terminated when the root mean square gradient fell below the 0.05. The initial and final energies of protein were calculated (in kcal/mol) by using the MMFF94X force field. Active site was selected, and ten different docked conformations were generated for both synthetic compound and kojic acid. Lowest energy conformation of

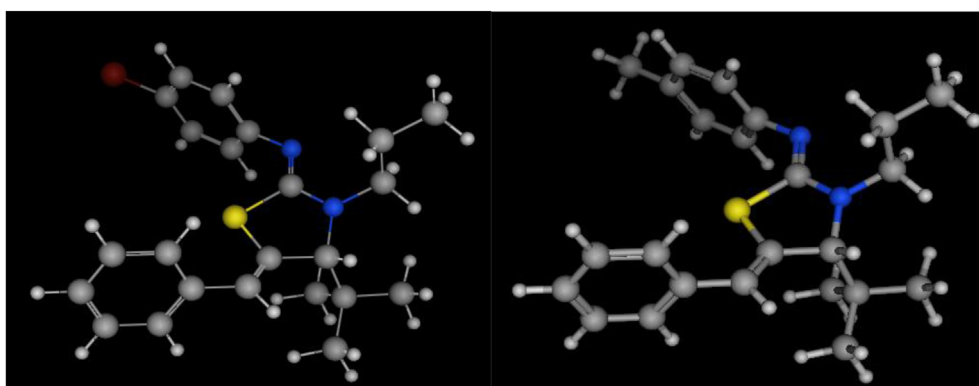
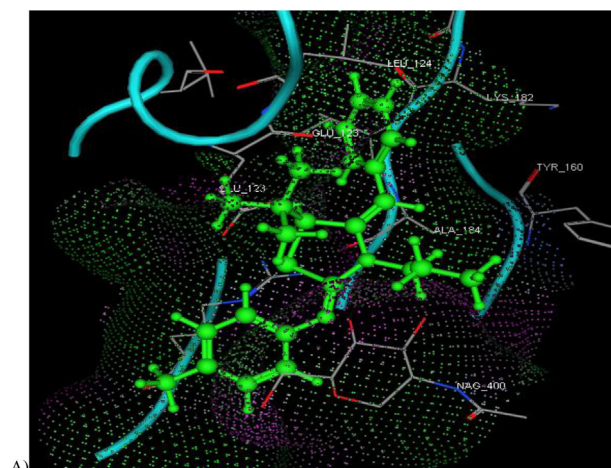
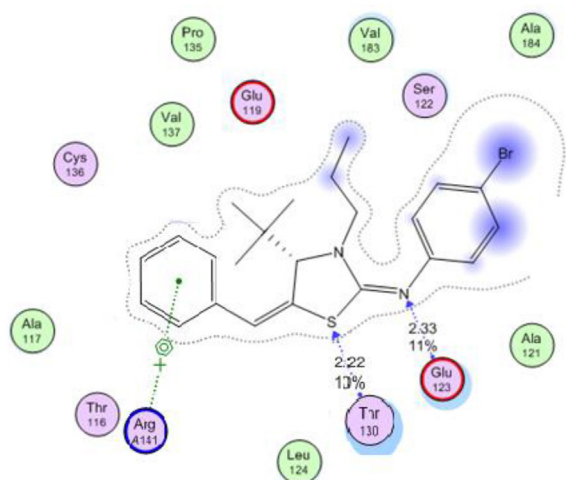


Figure 19. 3D lowest energy conformation of 4a & 4b generated in molecular docking studies.



A)



B)

Figure 21. Lowest energy 3D (A) & 2D (B) docked pose of compound **4b** in binding pocket of tyrosinase. In 2D structure the key amino acid residues are shown as sphere. Hydrogen bonds or arene-arene interactions are illustrated with dashed lines.

each compound was selected for binding pattern analysis. The minimized structure of protein was used as the template for docking.

Declarations

Author contribution statement

Syeda Aaliya Shehzadi: Conceived and designed the experiments; Performed the experiments.

Table 8. Crystallographic and structure refinement data for **4a**.

Compound	4a
Empirical formula	C ₂₄ H ₃₀ N ₂ S
Formula weight	378.56
T (K)	273(2)
Wavelength, λ (Å)	1.54178
Crystal system	Orthorhombic
Space group	P b c a
Crystal size (mm ³)	0.20 × 0.13 × 0.11
a (Å)	15.9557(4)
b (Å)	13.8445(3)
c (Å)	19.8008(5)
α (°)	90
β (°)	90
γ (°)	90
V (Å ³)	4373.97(18)
Z	8
F(000)	1632
Index ranges	-19 ≤ h ≤ 14 -16 ≤ k ≤ 16 -23 ≤ l ≤ 23
Reflections collected	25478
Independent reflections	3465 [R(int) = 0.0426]
Completeness to theta = 67.684°	99.6%
Absorption correction	
Max. and min. transmission	1.0000 and 0.87755
Refinement method	
Data/restraints/parameters	4131/0/249
Goodness-of-fit on F ²	1.044
Final R indices [I > 2σ(I)]	R1 = 0.0546, wR2 = 0.1349
R indices (all data)	R1 = 0.0477, wR2 = 0.1287
Largest diff. peak and hole (e.Å ⁻³)	0.379 and -0.855

Aamer Saeed, Pervaiz Ali Channar, Ifzan Arshad, Jim Simpson: Analyzed and interpreted the data.

Fouzia Perveen: Contributed reagents, materials, analysis tools or data; Wrote the paper.

Qamar Abbas: Performed the experiments.

Saima Kalsoom, Sammer Yousaf: Contributed reagents, materials, analysis tools or data.

Funding statement

This work was supported by the Higher Education Commission (HEC) Pakistan for research grant through Start-Up Research Grant (SRGP), project #1940.

Table 7. Summarised intermolecular interactions of **4a-b** and Kojic acid, inside the active site of human tyrosinase protein.

Entry	IC ₅₀ (μM)	H-bonding		Amino acids	Arene-π interactions Amino acids	π-π interactions Amino acids	Binding Energy (kcal/mol)
		Distance (°Å)	Score (%)				
4a	2.07 ± 0.87	3.04	17	ArgA141	PheA140	HisA186	-11.51
4b	1.15 ± 1.25	2.33, 2.22	11,10	Glu123, Thr100	ArgA141	-	-13.23
Kojic Acid	16.03 ± 1.27	1.77, 2.37, 3.68	41, 22, 11	Glu123 Lys182, Ala185,	-	-	-9.88

Data availability statement

Data associated with this study has been deposited at The Cambridge Crystallographic Data Centre (CCDC) under the accession number 2167819.

Declaration of interests statement

The authors declare no conflict of interest.

Additional information

No additional information is available for this paper.

Supplementary content related to this article has been published online at <https://doi.org/10.1016/j.heliyon.2022.e10098>.

References

- [1] F. Solano, S. Briganti, M. Picardo, G. Ghanem, Hypopigmenting agents: an updated review on biological, chemical and clinical aspects, *Pigment Cell Res* 19 (6) (2006) 550–571. <https://pubmed.ncbi.nlm.nih.gov/17083484/>.
- [2] S. Zolghadri, et al., A comprehensive review on tyrosinase inhibitors, *J. Enzym. Inhib. Med. Chem.* 34 (1) (2019) 279–309.
- [3] T.-S. Chang, An updated review of tyrosinase inhibitors, *Int. J. Mol. Sci.* 10 (6) (2009) 2440–2475.
- [4] S. Halaoui, et al., Fungal tyrosinases: new prospects in molecular characteristics, bioengineering and biotechnological applications, *J. Appl. Microbiol.* 100 (2) (2006) 219–232.
- [5] M.T. Khan, Novel tyrosinase inhibitors from natural resources - their computational studies, *Curr. Med. Chem.* 19 (14) (2012) 2262–2272.
- [6] S.Y. Seo, V.K. Sharma, N. Sharma, Mushroom tyrosinase: recent prospects, *J. Agric. Food Chem.* 51 (10) (2003) 2837–2853.
- [7] S. Halaoui, et al., Characterization of a new tyrosinase from *Pycnoporus* species with high potential for food technological applications, *J. Appl. Microbiol.* 98 (2) (2005) 332–343.
- [8] R.K. Sahu, et al., Promotion and computation of inhibitory effect on tyrosinase activity of herbal cream by incorporating indigenous medicinal plants, *Pakistan J. Biol. Sci.* 17 (1) (2014) 146–150.
- [9] S.Y. Lee, N. Baek, T.G. Nam, Natural, semisynthetic and synthetic tyrosinase inhibitors, *J. Enzym. Inhib. Med. Chem.* 31 (1) (2016) 1–13.
- [10] S.A. Shehzadi, et al., Zn(OTf)₂-Catalyzed synthesis of 2-alkynylazetidines and their ring expansion to functionalized 1,4,5,6-tetrahydropyridines, *Adv. Synth. Catal.* 360 (22) (2018) 4393–4401.
- [11] S.A. Shehzadi, et al., Zinc(II)-Catalyzed synthesis of propargylamines by coupling aldimines and ketimines with alkynes, *Eur. J. Org. Chem.* 2018 (1) (2018) 78–88.
- [12] I. Khan, A. Ibrar, S.A. Shehzadi, Building molecular complexity through transition-metal-catalyzed oxidative annulations/cyclizations: harnessing the utility of phenols, naphthols and 1,3-dicarbonyl compounds, *Coord. Chem. Rev.* 380 (2019) 440–470.
- [13] S.A. Shehzadi, A. Saeed, Cu(I)-catalyzed green synthesis of propargyl amines decorated with carbazole moiety by A³-coupling, *J. Chin. Chem. Soc.* 64 (7) (2017) 777–785.
- [14] S.A. Shehzadi, et al., Synthesis of highly functionalized 1,6-dihydropyridines via the Zn(OTf)₂-catalyzed three-component cascade reaction of aldimines and two alkynes (IA²-coupling), *Org. Biomol. Chem.* 16 (17) (2018) 3241–3247.
- [15] M.L. Barreca, et al., Discovery of 2,3-diaryl-1,3-thiazolidin-4-ones as potent anti-HIV-1 agents, *Bioorg. Med. Chem. Lett* 11 (13) (2001) 1793–1796.
- [16] S. Cuzzocrea, et al., Antiinflammatory effects of mercaptoethylguanidine, a combined inhibitor of nitric oxide synthase and peroxynitrite scavenger, in carrageenan-induced models of inflammation, *Free Radic. Biol. Med.* 24 (3) (1998) 450–459.
- [17] S.A. Shehzadi, et al., One-pot four-component synthesis of thiazolidin-2-imines using CuI/ZnII dual catalysis: a new class of acetylcholinesterase inhibitors, *Bioorg. Chem.* 84 (2019) 518–528.
- [18] M.T. Chhabria, et al., Thiazole: a review on chemistry, synthesis and therapeutic importance of its derivatives, *Curr. Top. Med. Chem.* 16 (26) (2016) 2841–2862.
- [19] C.B. Mishra, S. Kumari, M. Tiwari, Thiazole: a promising heterocycle for the development of potent CNS active agents, *Eur. J. Med. Chem.* 92 (2015) 1–34.
- [20] S. Nayak, S.L. Gaonkar, A review on recent synthetic strategies and pharmacological importance of 1,3-thiazole derivatives, *Mini Rev. Med. Chem.* 19 (3) (2019) 215–238.
- [21] M. Rezaei, et al., Evaluation of thiazolidinone derivatives as a new class of mushroom tyrosinase inhibitors, *Int. J. Biol. Macromol.* 108 (2018) 205–213.
- [22] Y.M. Ha, et al., Design and synthesis of 5-(substituted benzylidene)thiazolidine-2,4-dione derivatives as novel tyrosinase inhibitors, *Eur. J. Med. Chem.* 49 (2012) 245–252.
- [23] S.H. Kim, et al., Anti-melanogenic effect of (Z)-5-(2,4-dihydroxybenzylidene)thiazolidine-2,4-dione, a novel tyrosinase inhibitor, *Arch. Pharm. Res. (Seoul)* 36 (10) (2013) 1189–1197.
- [24] E. Bang, et al., Evaluation of the novel synthetic tyrosinase inhibitor (Z)-3-(3-bromo-4-hydroxybenzylidene)thiochroman-4-one (MHY1498) in vitro and in silico, *Molecules* 23 (12) (2018) 3307.
- [25] Y.K. Han, et al., Characterization of a novel tyrosinase inhibitor, (2R,4R)-2-(2,4-dihydroxyphenyl)thiazolidine-4-carboxylic acid (MHY384), *Biochim. Biophys. Acta* 1820 (4) (2012) 542–549.
- [26] H.J. Jung, et al., A novel synthetic compound, (Z)-5-(3-hydroxy-4-methoxybenzylidene)-2-iminothiazolidin-4-one (MHY773) inhibits mushroom tyrosinase, *Biosci., Biotechnol., Biochem.* 82 (5) (2018) 759–767.
- [27] S. Arshadi, et al., N-Propargylamines: versatile building blocks in the construction of thiazole cores, *Beilstein J. Org. Chem.* 13 (2017) 625–638.
- [28] V.A. Peshkov, et al., Tetrasubstituted 2-imidazolones via Ag(I)-Catalyzed cycloisomerization of propargylic ureas, *J. Org. Chem.* 76 (14) (2011) 5867–5872.
- [29] A. Ranjan, et al., An asymmetric alkylation/hydrothiolation cascade: an enantioselective synthesis of thiazolidine-2-imines from imines, acetylenes and isothiocyanates, *Chem. Commun.* 51 (75) (2015) 14215–14218.
- [30] A. Ranjan, et al., Base-mediated hydroamination of propargylamine: a regioselective intramolecular 5-exo-dig cycloisomerization en route to imidazole-2-thione, *Org. Lett.* 16 (21) (2014) 5788–5791.
- [31] J. Bernstein, et al., Patterns in hydrogen bonding: functionality and graph set analysis in crystals, *Angew. Chem. Int. Ed. Engl.* 34 (15) (1995) 1555–1573.
- [32] M.A. Spackman, D. Jayatilaka, Hirshfeld surface analysis, *CrystEngComm* 11 (1) (2009) 19–32.
- [33] M.N. Arshad, et al., Synthesis, crystal structures and spectroscopic properties of triazine-based hydrazone derivatives; a comparative experimental-theoretical study, *Molecules* 20 (4) (2015) 5851–5874.
- [34] M. Noreen, et al., Synthesis, density functional theory (DFT), urease inhibition and antimicrobial activities of 5-aryl thiophenes bearing sulphonylacamide moieties, *Molecules* 20 (11) (2015) 19914–19928.
- [35] Z. Ashraf, et al., Synthesis, kinetic mechanism and docking studies of vanillin derivatives as inhibitors of mushroom tyrosinase, *Bioorg. Med. Chem.* 23 (17) (2015) 5870–5880.
- [36] Z. Ashraf, et al., Design, synthesis and bioevaluation of novel umbelliferone analogues as potential mushroom tyrosinase inhibitors, *J. Enzym. Inhib. Med. Chem.* 30 (6) (2015) 874–883.
- [37] Z. Ashraf, et al., Kinetic and in silico studies of novel hydroxy-based thymol analogues as inhibitors of mushroom tyrosinase, *Eur. J. Med. Chem.* 98 (2015) 203–211.
- [38] F.A. Larik, et al., Design, synthesis, kinetic mechanism and molecular docking studies of novel 1-pentanoyl-3-arylthioureas as inhibitors of mushroom tyrosinase and free radical scavengers, *Eur. J. Med. Chem.* 141 (2017) 273–281.
- [39] W. Yi, et al., Synthesis and biological evaluation of novel 4-hydroxybenzaldehyde derivatives as tyrosinase inhibitors, *Eur. J. Med. Chem.* 45 (2) (2010) 639–646.
- [40] G. Sheldrick, SHELXT - integrated space-group and crystal-structure determination, *Acta Crystallogr. A* 71 (1) (2015) 3–8.
- [41] G. Sheldrick, Crystal structure refinement with SHELXL, *Acta Crystallogr. C* 71 (1) (2015) 3–8.
- [42] C.F. Macrae, et al., Mercury CSD 2.0 - new features for the visualization and investigation of crystal structures, *J. Appl. Crystallogr.* 41 (2) (2008) 466–470.
- [43] A. Spek, Structure validation in chemical crystallography, *Acta Crystallogr. D* 65 (2) (2009) 148–155.
- [44] L. Farrugia, WinGX and ORTEP for windows: an update, *J. Appl. Crystallogr.* 45 (4) (2012) 849–854.
- [45] Frisch, M.J., et al., *Gaussian 16 Rev. C.01*. 2016: Wallingford, CT.